

The Chocolate Chip Cookie Model: dust-to-metal ratio of H II regions

JIAFENG LU (卢家凤) ^{1,2} SHIYIN SHEN (沈世银) ^{1,3} FANG-TING YUAN (袁方婷) ^{1,3} AND QI ZENG (曾琪) ^{1,2}

¹Key Laboratory for Research in Galaxies and Cosmology, Shanghai Astronomical Observatory, Chinese Academy of Sciences, 80 Nandan Road, Shanghai 200030, People's Republic of China

²University of Chinese Academy of Sciences, 19A Yuquan Road, Beijing 100049, People's Republic of China

³Key Lab for Astrophysics, Shanghai, 200034, People's Republic of China

(Received; Revised; Accepted)

Submitted to APJL

ABSTRACT

Using a sample of face-on star-forming galaxies selected from the Sloan Digital Sky Survey, we statistically derive the typical optical depth τ_{cl} of individual H II regions based on the “Chocolate Chip Cookie” model of Lu et al. (2022). By binning galaxies into stellar mass and gas-phase metallicity bins and interpreting τ_{cl} as the dust to gas ratio (DGR) of H II regions, we further investigate the correlations among DGR and stellar mass, gas-phase metallicity respectively. We find that DGR increases monotonically with the stellar mass of galaxies. At a given stellar mass, DGR shows a linear correlation with the gas-phase metallicity, which implies a constant dust to metal ratio (DTM) of galaxies at a given stellar mass. These results adequately indicate that the DTM of galaxies is simply a function of their stellar masses. In terms of gas-phase metallicity, because of the mass-metallicity relation, DTM increases with increasing metallicity with a power-law index 1.45 in the low metallicity region, while remains constant at the high metallicity end.

Keywords: Disk galaxies(391)-Extinction(505)-Interstellar dust(836)-Interstellar dust extinction(837)

1. INTRODUCTION

Dust plays an important role in star formation and galaxy evolution. The properties of dust in galaxies, particularly the dust-to-gas ratio (DGR) and dust-to-metal ratio (DTM) have been intensively studied through statistical scaling relations (Lisenfeld & Ferrara 1998; Hirashita et al. 2002; Draine et al. 2007; Galametz et al. 2011; Zafar & Watson 2013; Rémy-Ruyer et al. 2014; De Vis et al. 2019; Wiseman et al. 2017; Kahre et al. 2018). Dust evolution models show that the growth of dust grains increases DTM (Mattsson et al. 2012), while dust destruction performs in the opposite way (Draine & Salpeter 1979). Therefore, in observation, the DGR or DTM as a function of metallicity provides an effective constraint on dust evolution mechanisms. Early studies have suggested a linear relation between DGR and metallicity, or a constant DTM (Issa et al. 1990; Lisenfeld & Ferrara 1998), for a wide range of galaxies, which was explained by the ineffectiveness of grain growth and destruction (Hirashita 1999; Edmunds 2001). A constant DTM is also assumed in many semi-analytic models and hydro-dynamical simulations (Silva et al. 1998; James et al. 2002; Clark et al. 2016; Yajima et al. 2015; Camps et al. 2015; Somerville et al. 2012;

Ma et al. 2019; Katz et al. 2019). In recent studies, a variable metallicity dependent DTM has been widely presented by infrared (IR) observations, especially for galaxies with low metallicity (for example Rémy-Ruyer et al. 2014; De Vis et al. 2017, 2019). However, selection effects or uncertainties could result in different observational trends because of the small sample size of a few hundred galaxies (Mattsson et al. 2014).

The large galaxy samples in optical survey is more suitable for statistical study. However, it is not straightforward to derive the DGR or DTM from the optical observations alone. With spectroscopic observations, the gas-phase metallicity of star forming galaxies (SFG) can be easily derived from the emission lines of H II regions (for example Tremonti et al. 2004). Therefore, if we can have a implicit probe of the average amount of dust (i.e. optical depth) of the H II regions of SFG using optical observations, we could study the dependence of DGR (or DTM) on the other physical properties of galaxies statistically with a large sample. However, the statistical estimation of the average amount of dust (optical depth) of H II regions in extra-galactic galaxies is nontrivial. First of all, we can not get the observational constraint on the optical depth of H II regions through the reddening of the emission

lines directly. The emission lines of H II regions are not only extinguished by the dust layer of themselves, but also extinguished by the foreground ISM along the line-of-sight. Moreover, considering the clumpy distribution of H II regions, along the line-of-sight, especially when the disk galaxies are highly-inclined, there will be an inter-covering effect of H II regions, which will certainly result in a biased estimation of the average dust extinction of H II regions.

Recently, Lu et al. (2022) have provided a framework of the dust configuration of disk galaxies named as the ‘‘Chocolate Chip Cookie’’ (hereafter CCC) model, in which the clumpy nebular regions are embedded in a diffuse stellar/ISM disk, like chocolate chips in cookies. In this model, the average optical depth of individual H II regions τ_{cl} is a model parameter, which can be well constrained because both the foreground ISM dust extinction and the mutual attenuation of H II clumps have been carefully considered. Moreover, as we will show in Section 2, for face-on galaxies, the derivation of the optical depth of individual H II regions could be even simplified. That is to say, using the CCC model, we can obtain the typical optical depth of the H II regions and then estimate the DTM for a given sample of star-forming galaxies based on the optical observation data alone.

In this work, we aim to derive the average optical depth of individual H II regions, τ_{cl} , via an approximation of CCC model with a sample of face-on SFG in the Sloan Digital Digital Sky Survey (SDSS). Then, we explore the dependence of τ_{cl} on the stellar mass and gas-phase metallicity of galaxies, which gives us more details about the variations of DTM and puts constraints on the possible physical mechanisms of these variations.

The outline of this paper is as follows. In Section 2, we present a face-on SFG sample and show their dust reddening features. In Section 3, we introduce a method to interpret DTM as a function of τ_{cl} and gas-phase metallicity. Then, we use the simplified ‘‘CCC model’’ to derive τ_{cl} for different sub-sample of galaxies. We present our main results in Section 4 and make discussions on the DTM of SFGs in Section 5. Finally, we make a summary in Section 6.

2. DATA: FACE-ON DISK GALAXY SAMPLE

In this study, we use the SFG sample of (Lu et al. 2022), which was selected from the spectroscopic main sample galaxies of the SDSS using the BPT diagram applied with the criteria of Kauffmann et al. (2003a) and requiring the signal-to-noise ratio (S/N) of each emission lines larger than 3. Unlike the Milky-Way like (MW-like) galaxies studied in Lu et al. (2022), we apply the CCC model to galaxies in a much large stellar mass range ($9 < \log M_* < 11$, where M_* represents the stellar mass in unit of solar mass). Moreover, we further select the face-on SFGs with an axis ratio $b/a > 0.8$ to simplify the CCC model so that the constraints

on the optical depth of the H II regions can be more explicitly obtained (see Section 3 for detail). We therefore finally obtain a sample of 25,573 face-on SFGs within the stellar mass range $9 < \log M_* < 11$. In our sample, the gas-phase metallicity ($12 + \log(\text{O}/\text{H})$) is obtained from the MPA-JHU database¹, following Tremonti et al. (2004).

Following the same method as Lu et al. (2022), we first obtain the stellar reddening E_s and the emission line reddening E_g for each sample galaxies. In short, the stellar reddening E_s is obtained via the stellar population synthesis code STARLIGHT (Cid Fernandes et al. 2005) with the BC03 single stellar population (Bruzual & Charlot 2003). The emission line reddening E_g is obtained via Balmer decrement.

We show the resulted M_* - E_s and M_* - E_g density distribution in Figure 1. The medians of E_g and E_s in stellar mass bins of 0.2 dex are connected with black solid lines, while the black dashed lines are the contours that enclose 68 percentiles of E_g or E_s distribution. Moreover, at a given stellar mass bin, we further divide the sample galaxies into 3 metallicity bins with equal number of galaxies and calculate their median E_s and E_g , respectively, which are shown as the color dots in Figure 1. We also estimate the uncertainties of the median E_g and E_s in each stellar mass and metallicity bin using the formula $\sqrt{\frac{\pi}{2}} \frac{\sigma}{\sqrt{n}}$, where σ is the standard deviation of E_s or E_g distribution and n is the number of galaxy sample in each bin. These uncertainties are also plotted in Figure 1 as the errorbar on each color dot and will be used to estimate the uncertainties τ_{cl} in Section 3. As shown in Figure 1, E_s shows a plateau at 0.1 for low stellar mass ($\log M_* < 9.5$), then increases slightly from 0.1 to 0.15 with stellar mass in the range of $9.5 < \log M_* < 11$, while E_g increases monotonically from 0.1 to 0.5 with stellar mass. At given stellar mass, both E_g and E_s further increase with the increasing of metallicity.

It is important to note that our measurement of E_g does not directly represent the dust extinction (optical depth) of the H II region itself. However, with these two measurements (E_g and E_s), as we will show in Section 3, our CCC model can easily and robustly estimate τ_{cl} for face-on SFGs.

3. METHOD: DERIVING OPTICAL DEPTH OF INDIVIDUAL H II REGIONS

Before deriving the typical optical depth τ_{cl} of individual H II regions, we first discuss how τ_{cl} could represent the dust abundance of H II regions. We assume a simple model of a sphere with a dust shell for H II regions. For the inner sphere, the gas is fully ionized, and we assume there is no dust. In the outer shell, the dust is uniformly mixed with the neutral gas. The metallicity is assumed to be the same for the ionized

¹ <https://www.mpa.mpa-garching.mpg.de/SDSS/DR7/oh.html>

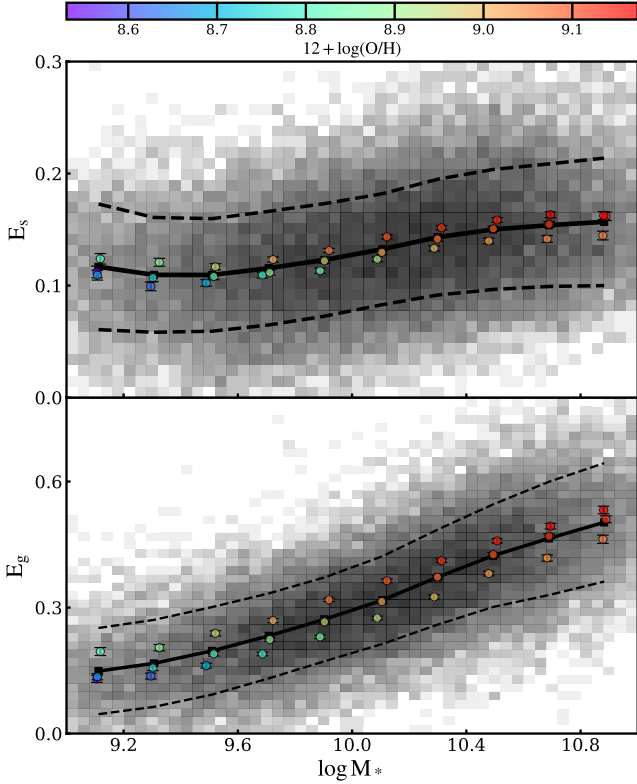


Figure 1. The stellar reddening E_s (top panel) and nebular reddening E_g (bottom panel) as a function of stellar mass for face-on SFGs. In each panel, the black line represents the median E_s (or E_g), where the two black dashed lines are the 16 and 84 percentiles of E_s (or E_g) respectively. For each stellar mass bin, the colored dots further show the median E_s (or E_g) of three different metallicity bins, which are color-coded according to the color-bar plotted on the top of the figure.

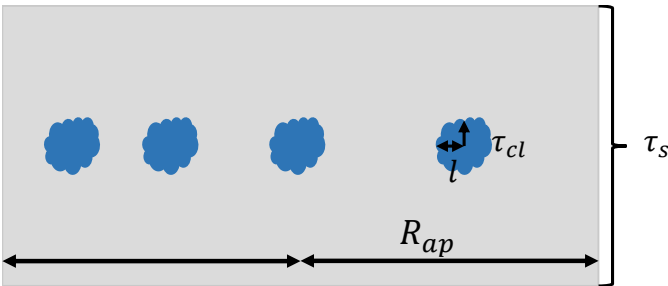


Figure 2. Sketch diagram of simplified CCC model for a face-on disk galaxy inside a fiber aperture (radius R_{ap}), where a single layer of individual H II regions (blue clouds, intrinsic optical depth τ_{cl} and dust shell thickness l) are sparsely embedded in the middle of a thick ISM disk (gray background, total optical depth τ_s along the line-of-sight).

gas of the inner sphere and the neutral gas of the outer shell. With this toy model, We write τ_{cl} in the form

$$\tau_{cl} = \kappa_V \rho_{dust} l, \quad (1)$$

where ρ_{dust} is the volume density of the dust particles in the outer shell, l is the thickness of the dust shell, κ_V is the dust absorption coefficient. By linking ρ_{dust} to the DTG and neutral gas volume density of shell ρ_{gas} , we get

$$\tau_{cl} = \kappa_V \rho_{gas} l \cdot DTG. \quad (2)$$

In equation 2, ρ_{gas} and l parameterize the basic geometric properties of shell of H II regions, κ_V characterizes the physical properties of dust particles.

Here, we assume that ρ_{gas} , l and κ_V are all independent of their host galaxies. Considering the the average electron density and size distribution of H II regions are similar for all types of local SFGs (Oey et al. 2003; Liu et al. 2013; Santoro et al. 2022) and the inner ionized sphere and dust shell are both a part of H II complex, the assumption is somewhat reasonable. We therefore get $\tau_{cl} \propto DTG$. With this assumption, we will use τ_{cl} to represent the DTG of galaxies and then study its dependence on other physical properties of galaxies.

The DTG can be further written as the product of DTM (denoted as ζ) and metallicity Z . In this study, we use the gas-phase metallicity estimated by Tremonti et al. (2004), which is defined as the logarithmic abundance ratio of oxygen to hydrogen and denoted as $12 + \log(O/H)$. Therefore, in logarithmic space, the relation between ζ and τ_{cl} is

$$C + \log \zeta = \log \tau_{cl} - \log(O/H). \quad (3)$$

where the constant term C represents the unknown and unrelated constant factors assumed in this study (e.g. κ_V, ρ_{gas}, l in Equation 2).

In Lu et al. (2022), we have presented a two-component dust geometry model for disk galaxies, the CCC model, where the H II regions (“chocolate chips”) are embedded in a continuously distributed ISM disk (“cookie”). In the CCC model, the diffuse ISM is assumed to be uniformly mixed with the stellar component, whereas the H II regions are clumpy and distributed in a much thinner disk.

For face-on galaxies, this model can be further simplified to a scenario in which a single layer of H II regions sparsely embedded in the middle of a thick ISM disk, as illustrated in Figure 2. In Lu et al. (2022), we have obtained the cross section of H II regions in the central region of MW-like galaxies is 0.84 kpc^{-1} (defined as the average number of H II regions in the central line-of-sight) and a very low thickness of the H II disk (scale-height $\sim 0.1 \text{ kpc}$). For face-on MW-like galaxies, the covering factor of the H II regions inside a fiber aperture is about 0.1 so that the obscuration of the H II regions to the stars is negligible. In this study, we assume all SFGs have a

dust geometry configuration similar to MW-like galaxies and make two reasonable assumptions for all face-on SFGs: (1) there is at most one H II region along any single line-of-sight; (2) the covering factor of H II regions is very low.

With these two assumptions, the stellar emission is only attenuated by the ISM dust and the H II nebular emission is attenuated by the ISM dust and the dust shell of the H II region itself. Since the ISM dust is assumed to be uniformly mixed with stellar population in the CCC model, the stellar attenuation and the emission line attenuation can be simplified as the uniform mixture model and the screen model respectively, which have also been discussed in [Lu et al. \(2022\)](#). Besides, as the typical size of H II regions is much smaller than the scale-height of the stellar disk, the optical depth of the foreground ISM dust of H II regions can be approximated by the half of the total optical depth of ISM dust. Finally, the stellar and nebular reddening are then both the functions of optical depths:

$$\begin{aligned} E_s &= 2.5 \log\left(\frac{\tau_{s,B}}{\tau_{s,V}} \frac{1 - e^{-\tau_{s,V}}}{1 - e^{-\tau_{s,B}}}\right) \\ E_g &= 1.086(\tau_{g,H\beta} - \tau_{g,H\alpha}) \\ \tau_g &= \frac{\tau_s}{2} + \tau_{cl}. \end{aligned} \quad (4)$$

where τ_s is the total optical depth of ISM dust (see Figure 2), τ_g is the total optical depth of the nebular region along the line-of-sight and τ_{cl} is the optical depth of individual H II regions only.

Based on Equation 4, τ_s and τ_{cl} ² can be derived from the observed E_g and E_s by assuming an extinction curve. Following [Lu et al. \(2022\)](#), we assume a power law attenuation curve with the typical total to selective extinction $R_V = 3.1$ ([Li et al. 2017](#); [Fitzpatrick et al. 2019](#)):

$$\frac{A_\lambda}{A_V} = \left(\frac{\lambda}{5500\text{\AA}}\right)^{-1.32} \quad (5)$$

As we have shown in [Lu et al. \(2022\)](#), when given a certain geometry of dust and stars, this extinction curve can reproduce the classical attenuation curve of Calzetti law ([Calzetti et al. 2000](#)).

It should be noted that the CCC model deduces τ_{cl} of individual H II regions from a statistical perspective. Moreover, instead of deriving τ_{cl} for each individual galaxy using Equation 4, we take the median E_g and E_s for a sample of galaxies with similar physical properties and calculate their typical τ_{cl} values. Meanwhile, the uncertainties of τ_{cl} are derived by propagating the uncertainties of E_g and E_s . In other words, the motivation of this paper is to study the τ_{cl} of SFGs in a statistical sense, rather than focusing on the specific values of τ_{cl} for any individual galaxies.

² In this paper, if not explicitly specified, the optical depth is defined in the default wavelength V-band.

4. RESULTS

In Section 2, we divide the face-on SFGs into 10 stellar mass bins with bin width of 0.2 dex, and then the galaxies at given stellar mass bin are further divided into sub-samples of 3 gas-phase metallicity bins with equal numbers. In this section, we take these sub-samples and explore the variation of τ_{cl} as function of stellar mass M_* and metallicity ($12 + \log(\text{O}/\text{H})$) of host galaxies using the simplified CCC model outlined in Section 3.

We first show the M_* -Z relation of all face-on SFGs with small dots in the top-left panel of Figure 3. We show the median $12 + \log(\text{O}/\text{H})$ as a function of stellar mass with the solid curve, which is parameterized by a quadratic function following [Tremonti et al. \(2004\)](#)³:

$$\begin{aligned} 12 + \overline{\log(\text{O}/\text{H})}(M_*) &= \\ &- 0.114(\log M_*)^2 + 2.534 \log M_* - 4.978. \end{aligned} \quad (6)$$

Besides, the subsamples of galaxies in 30 stellar mass and metallicity bins are shown by circle dots in this panel, whose color codes the τ_{cl} values of each subsample. As can be seen, more massive and more metal rich galaxies have systematically higher τ_{cl} values, ranging from $\tau_{cl} \sim 0.05$ for the least massive and metal poor galaxies ($\log M_* \sim 9$, $12 + \log(\text{O}/\text{H}) \sim 8.5$) to $\tau_{cl} \sim 0.8$ for the most massive and metal rich galaxies ($\log M_* \sim 11$, $12 + \log(\text{O}/\text{H}) \sim 9.2$).

To show the dependence of τ_{cl} on stellar mass and metallicity clearly, we plot τ_{cl} as a function of M_* in the top-right panel of Figure 3, where the median $12 + \log(\text{O}/\text{H})$ of each sample galaxies are color coded. We first show the median τ_{cl} of sample galaxies in 10 stellar mass bins irrespective of their metallicity as big squares. The τ_{cl} of sample galaxies in 30 stellar mass and metallicity bins are then shown as circle dots connected by dotted lines. For clarity, we only show the uncertainties of τ_{cl} for 10 stellar mass bins. For the global median τ_{cl} in 10 M_* bins (squares), we see that $\overline{\tau_{cl}}$ increases monotonically with stellar mass. Following the M_* -Z relation, we also parameterize the M_* - $\overline{\tau_{cl}}$ relation with a quadratic function and get the best fit

$$\log \overline{\tau_{cl}}(M_*) = -0.343(\log M_*)^2 + 7.54 \log M_* - 41.531, \quad (7)$$

which is shown as the black solid curve in this panel. Besides the M_* -Z degeneracy, again, we see a clear second-order dependence of τ_{cl} on metallicity at given stellar mass: higher Z galaxies have higher τ_{cl} .

To show the second order dependence of τ_{cl} on Z more clearly, we plot the residual and their error of the M_* - τ_{cl} relation ($\Delta \log \tau_{cl}$) as function of the residual of the M_* -Z relation

³ This fitting formula is obtained using `curve_fit` module in `scipy` library of Python3, and is very similar to that of [Tremonti et al. \(2004\)](#).

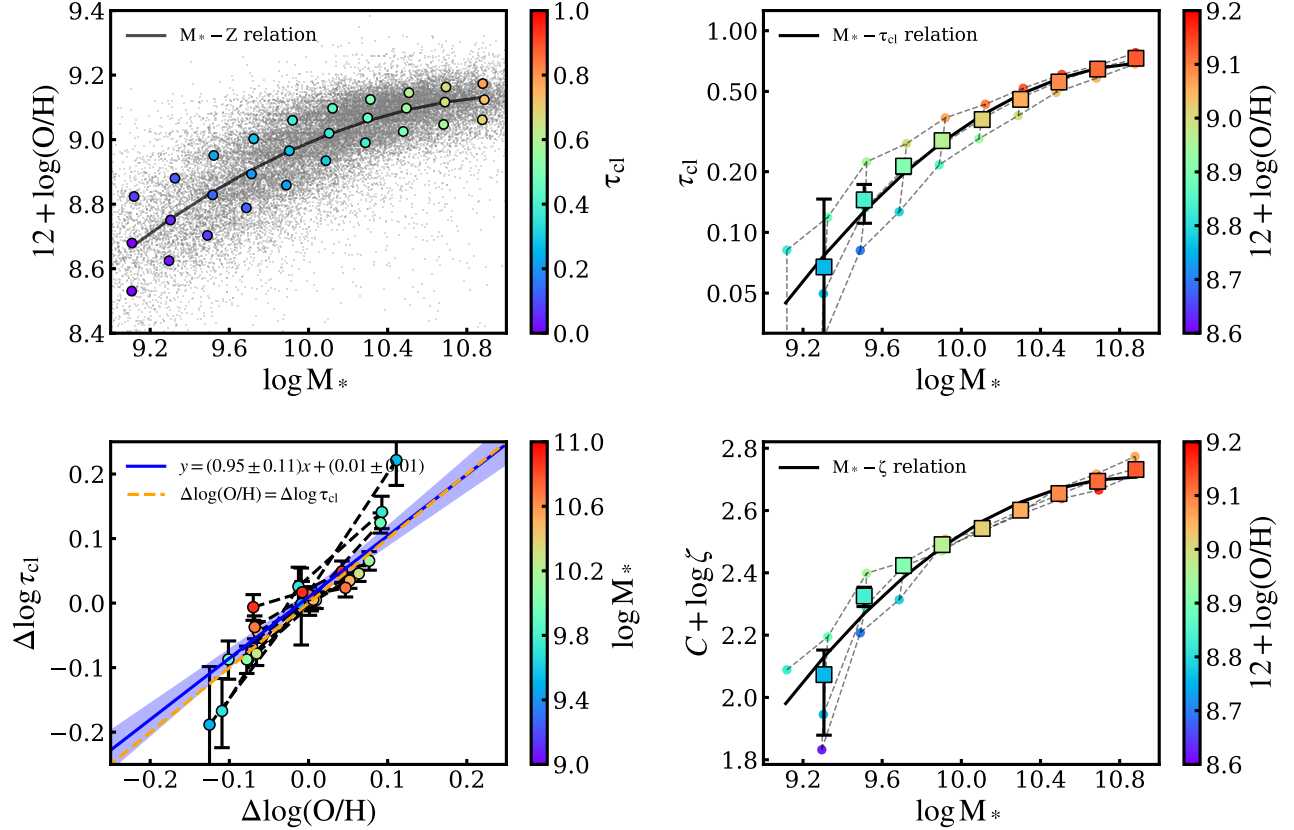


Figure 3. The dependence of τ_{cl} on stellar mass M_* and metallicity $12 + \log(\text{O}/\text{H})$. Top-left panel: $M_* - Z$ relation, and τ_{cl} is color-coded. The circles represent the 30 sub-sample of galaxies in M_* and Z bins, while the small black dots in background are all sample galaxies. The solid curve is the fitted $M_* - Z$ relation of Equation 6. Top-right panel: $M_* - \tau_{\text{cl}}$ relation, and metallicity color-coded. The dots connected by dotted lines represent the sub-sample of galaxies in 30 stellar mass and metallicity bins, while the squares show the median τ_{cl} values in 10 stellar mass bins irrespective of metallicity. The solid curve is the fitted $M_* - \tau_{\text{cl}}$ relation of Equation 7. Bottom-left panel: the residual $\Delta \log \tau_{\text{cl}} - \Delta \log(\text{O}/\text{H})$ relation color-coded with the M_* of different stellar mass bin. The galaxy bins with the same stellar mass are connected by black dashed lines. The best fit and the confidence level of 1σ are shown by the blue solid curve and shadowed regions. The dashed orange diagonal line ($\Delta \log \tau_{\text{cl}} = \Delta \log(\text{O}/\text{H})$) is plotted for comparison. Bottom-right panel: $M_* - \zeta$ relation color-coded with the metallicity. The data points are the same as that of the upper left panel. The solid curve follows Equation 9.

($\Delta \log(\text{O}/\text{H})$) in the bottom-left panel of Figure 3. In specific, these two residuals are defined as

$$\begin{aligned} \Delta \log(\text{O}/\text{H}) &= \log(\text{O}/\text{H}) - \overline{\log(\text{O}/\text{H})}(M_*), \\ \Delta \log \tau_{\text{cl}} &= \log \tau_{\text{cl}} - \overline{\log \tau_{\text{cl}}}(M_*) \end{aligned} \quad (8)$$

where $\overline{\log(\text{O}/\text{H})}(M_*)$ and $\overline{\log \tau_{\text{cl}}}(M_*)$ are defined by Equations 6 and 7, respectively. We also fit the global trend with a linear relation. The relation and its confidence level of 1σ are also plotted with blue solid line and shadowed regions in the bottom-left panel of Figure 3. As can be seen, after subtracting the $M_* - \overline{\tau_{\text{cl}}}$ relation and $M_* - \overline{Z}$ relation, $\Delta \log \tau_{\text{cl}}$ roughly shows a linear relation with $\Delta \log(\text{O}/\text{H})$ for all M_* bins with a slope of 1. According to Equation 3, this equivalence im-

plies that the DTM (ζ) of galaxies with different metallicity are roughly a constant at given stellar mass.

To further investigate the results shown above, we plot ζ (defined as Equation 3) as a function of M_* only in the bottom-right panel of Figure 3, color coded according to the metallicity. Following the top-right panel, we show the sample galaxies in 10 stellar mass bins irrespective of their metallicity as big squares and these sub-samples in 30 stellar mass and metallicity bins as circle dots connected by dotted lines. As can be seen, ζ almost shows no second-order dependence on metallicity for most stellar mass bins ($\log M_* > 9.8$). For these few low mass bins, considering the uncertainties of ζ there, we believe ζ is also largely independent of metallicity. Even if there is a correlation, the correlation should be very weak. Since ζ is only a function of stellar mass, we provide

an analytic expression of that function. Rather than fitting the data points in the bottom-right panel, we can also obtain it by the combination of Equations 3, 6, 7 and 8,

$$\begin{aligned} C + \log \zeta &= \log \overline{\tau_{\text{cl}}}(\overline{M}_*) - \overline{\log(\text{O}/\text{H})}(\overline{M}_*) \\ &= -0.229(\log M_*)^2 + 5.006 \log M_* - 24.553. \end{aligned} \quad (9)$$

We plot this quadratic function as the solid curve in this panel. As can be seen, this derived analytic formula matches the data points very well.

From the plots shown above, we arrive at the main finding of this study: the DTM of a galaxy is a unique function of the stellar mass of its host galaxy. This finding has important implications for the time-scale of dust particle evolution, which will be further discussed in Section 5.2.

5. DISCUSSION

Most of the studies on dust evolution model focus on the dependence of ζ on metallicity (Lisenfeld & Ferrara 1998; Hirashita et al. 2002; Draine et al. 2007; Galametz et al. 2011; Zafar & Watson 2013; Rémy-Ruyer et al. 2014; De Vis et al. 2019; Wiseman et al. 2017; Kahre et al. 2018). The process of dust evolution consists of the dust production and destruction. The dust production is mainly motivated by dust formation in stellar winds and supernovae and grain growth in ISM. The dust destruction is mainly related to star formation depletion, thermal sputtering and supernova destruction. Besides, gas inflows and outflows also affect the amount of dust. Among these mechanisms, grain growth increases ζ while dust destruction have the opposite effect. If there are no grain growth and dust destruction, the ζ is a constant that depends on the yield of dust in stellar winds and supernovae. When there is a balance between dust grain growth and destruction, ζ is also a constant (i.e. De Vis et al. 2017; Mattsson et al. 2012). On the other hand, in dense and metal rich environments (e.g. in the inner regions of molecular clouds), the dust growth effect outweighs the destruction of dust particles, we would expect that ζ will increase with metallicity. In this paper, we propose that the stellar mass of host galaxy plays a more fundamental role in ζ of H II regions. In this Section, we first discuss the ζ -Z relation implied by M_* - ζ relation in our study (Section 5.1) and then explore possible physical mechanisms behind the M_* - ζ relation we propose (Section 5.2).

5.1. ζ -Z relation

Many studies have discussed the dependence of ζ on Z (e.g. Silva et al. 1998; James et al. 2002; Clark et al. 2016; Yajima et al. 2015; Camps et al. 2015; Somerville et al. 2012; Ma et al. 2019; Katz et al. 2019). To have a good comparison of our study with earlier results, we also explore the dependence of ζ on Z only. In specific, we divide our sample SFGs into

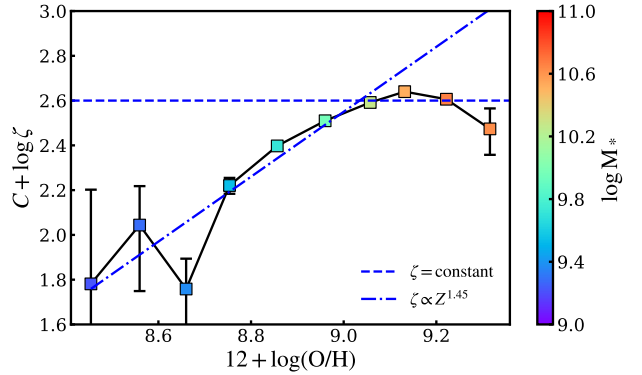


Figure 4. The dependence of $\log \zeta$ on $12 + \log(\text{O}/\text{H})$ with stellar mass color-coded, where the $\log \zeta$ is interpreted by $\log \tau_{\text{cl}} - \log(\text{O}/\text{H})$. The dot-dashed line has a slope of 1.45 and the dashed line represent the DTM is a constant.

10 metallicity bins in the range of $8.4 < 12 + \log(\text{O}/\text{H}) < 9.4$ with bin-width of 0.1 dex and then calculate the median τ_{cl} of the sample galaxies in each metallicity bin. Following Equation 3, we calculate ζ and then show its dependence on metallicity ($12 + \log(\text{O}/\text{H})$) in Figure 4, where the median $\log M_*$ of sample galaxies in each metallicity bin is color coded. We see that ζ increases monotonically with $\log(\text{O}/\text{H})$ at low metallicity range ($12 + \log(\text{O}/\text{H}) < 9.0$). At high metallicity end ($12 + \log(\text{O}/\text{H}) > 9.0$), ζ is roughly a constant. Such a trend has been reported in early studies (e.g. Rémy-Ruyer et al. 2014).

For more quantitative comparisons, we over-plot two suggested ζ -Z relations in the literature in Figure 4. One is the relation $\zeta \sim \text{constant}$ (Issa et al. 1990; Lisenfeld & Ferrara 1998) represented by the dashed line, where the intercept has been adjusted to fit the observed $\log \zeta$ at high metallicity. The other is the non-linear relation $\zeta \propto Z^{1.45}$ (e.g. De Vis et al. 2019; Li et al. 2019). This relation is shown by the dot-dashed line and the intercept also has been adjusted to fit the observed ζ -Z relation at low metallicity. As can be seen, these two known relations agree well with our results at low and high metallicity parts respectively.

According to the dependence of τ_{cl} on the two dimensional M_* and Z bins shown in the top-right panel of Figure 3, the slope of 1.45 between $\log \zeta$ and $\log(\text{O}/\text{H})$ at the low metallicity end shown in Figure 4 is more of the relation between τ_{cl} and M_* , which also can be clearly viewed from the color (stellar mass) of data points. At high metallicity end, M_* -Z relation becomes flat and M_* - τ_{cl} relation for high mass (metallicity) galaxies also becomes flat. As a result, ζ is a constant. In summary, in our study, the observed ζ -Z relation is a joint result of the M_* -Z (Equation 6) and M_* - ζ (Equation 9) relation.

5.2. Physical implications of M_* - ζ relation

The M_* - ζ relation we have derived have important physical implications on the assembly history of different components (e.g. stellar population, metal, dust) of galaxies.

The M_* - Z relation of local SFGs could be a result of higher surface density of more massive disk galaxies (Chang et al. 2010; Belfiore et al. 2017). Moreover, the star formation history of present-day galaxies shows a “downsizing” behavior, where the stars in more massive galaxies tend to be formed earlier and over a shorter time-span (Neistein et al. 2006). Therefore, the higher Z of more massive galaxies could also be a result of the higher star formation efficiency at higher redshift, when the surface gas density of galaxies is averagely higher (Fu et al. 2009). In general, the mass assembly history of galaxies is in the order of a few Gyrs, which is much longer than the dust grain growth time-scale in molecular clouds ($\sim 10^7 - 10^8$ year (Galliano 2022)). Therefore, considering that more massive galaxies assemble their metals earlier and the shorter dust grain growth time-scale in higher metallicity regions, it is natural that more massive galaxies have a higher ζ today.

On the other hand, the higher metallicity of more massive galaxies are possibly related to their deeper gravitational potential, where the outflows are suggested to be more difficult to escape from the host galaxy (Chang et al. 2010; Chisholm et al. 2017). Considering heavier mass of metal particles, for both the momentum and energy driven outflows, the metal particles naturally have lower outflow velocity and outflow rate than that of gas (Pandya et al. 2021). Predictably, the outflow fraction of dust grains would be even smaller than that of metal particles, as the dust grains are much heavier than metal particles. Therefore, the outflow scenario also provides a reasonable explanation to the lower Z and ζ in less massive galaxies, where the outflow is more prominent.

At a given stellar mass, our study shows that ζ is independent of gas-phase metallicity. This phenomena is possibly related to the physical condition and lifetime of H II regions. For the out layer of H II regions (or diffuse molecular cloud environments), the time-scale of dust growth (~ 100 Myr (Galliano 2022)) is much longer than the lifetime of H II regions (~ 10 Myr), and the temperature ($\sim 10^4 K$) there is a large offset from the requirement of dust sputtering or sublimation ($\sim 10^6 K$). Besides, the dust destruction effect by supernova can also be neglected since living OB stars are needed for H II regions. Therefore, ζ has not enough time to evolve during the short lifetime of H II regions. On the other hand, for galaxies at given stellar mass, the linear correlation between metallicity and optical depth is probably related to the stochastic feeding (e.g. metal-poor gas accretion) of SFG, which is a transient process and has been used to explain the local anti-correlation between star formation rate(SFR) and gas-phase metallicity (Sánchez Almeida

& Sánchez-Menguiano 2019). In this scenario, the stochastic feeding of metal-poor gas in short time-scale does not change either the total amount of metal or dust, that is, this kind of inflow causes a simultaneous decrease of both metallicity and DTG (τ_{cl}) and therefore does not affect ζ .

6. SUMMARY

In this study, by applying a simplified version of the Chocolate Chip Cookie model of Lu et al. (2022) on a sample of face-on star-forming galaxies selected from SDSS, we obtain the typical dust optical depth τ_{cl} of the H II regions for galaxies in different stellar mass and gas-phase metallicity bins. By investigating the dependence of τ_{cl} on M_* and Z and linking τ_{cl} to DTG of galaxies, we generate the following conclusions on DTG and DTM of star-forming galaxies.

We find that τ_{cl} increases with M_* faster than Z so that DTM ($\zeta \sim \tau_{cl}/Z$) increases with M_* of galaxies. At a given stellar mass, the residual $\Delta \log \tau_{cl}$ is linearly correlated with $\Delta \log(O/H)$, implying a constant ζ . Our results show that the stellar mass of galaxies is the first parameter in the DTM- Z relation of galaxies, like in many other scaling relations(e.g. Shen et al. 2003; Kauffmann et al. 2003b; Peng et al. 2010). The ζ - Z relation discussed in literature is a joint result of the M_* - ζ and M_* - Z relation.

ACKNOWLEDGMENTS

We thank the anonymous referee for the helpful and constructive comments that improve the paper. This work is supported by the National Natural Science Foundation of China (No. 12073059 & No. U2031139), the National Key R&D Program of China (No. 2019YFA0405501), an the Program of Shanghai Academic/Technology Research Leader (22XD1404200). We also acknowledge the science research grants from the China Manned Space Project with NO. CMS-CSST-2021-A04, CMS-CSST-2021-A07, CMS-CSST-2021-A08, CMS-CSST-2021-A09, CMS-CSST-2021-B04. F.T.Y. acknowledges support by the Funds for Key Programs of Shanghai Astronomical Observatory (No. E195121009) and the Natural Science Foundation of Shanghai (Project Number: 21ZR1474300).

Funding for the SDSS and SDSS-II has been provided by the Alfred P. Sloan Foundation, the Participating Institutions, the National Science Foundation, the U.S. Department of Energy, the National Aeronautics and Space Administration, the Japanese Monbukagakusho, the Max Planck Society, and the Higher Education Funding Council for England. The SDSS Web Site is <http://www.sdss.org/>.

The SDSS is managed by the Astrophysical Research Consortium for the Participating Institutions. The Participating Institutions are the American Museum of Natural History, Astrophysical Institute Potsdam, University of Basel, University of Cambridge, Case Western Reserve University, University of Chicago, Drexel University, Fermilab, the Institute for

Advanced Study, the Japan Participation Group, Johns Hopkins University, the Joint Institute for Nuclear Astrophysics, the Kavli Institute for Particle Astrophysics and Cosmology, the Korean Scientist Group, the Chinese Academy of Sciences (LAMOST), Los Alamos National Laboratory,

the Max-Planck-Institute for Astronomy (MPIA), the Max-Planck-Institute for Astrophysics (MPA), New Mexico State University, Ohio State University, University of Pittsburgh, University of Portsmouth, Princeton University, the United States Naval Observatory, and the University of Washington.

REFERENCES

- Belfiore, F., Maiolino, R., Tremonti, C., et al. 2017, *MNRAS*, 469, 151, doi: [10.1093/mnras/stx789](https://doi.org/10.1093/mnras/stx789)
- Bruzual, G., & Charlot, S. 2003, *MNRAS*, 344, 1000, doi: [10.1046/j.1365-8711.2003.06897.x](https://doi.org/10.1046/j.1365-8711.2003.06897.x)
- Calzetti, D., Armus, L., Bohlin, R. C., et al. 2000, *ApJ*, 533, 682, doi: [10.1086/308692](https://doi.org/10.1086/308692)
- Camps, P., Misselt, K., Bianchi, S., et al. 2015, *A&A*, 580, A87, doi: [10.1051/0004-6361/201525998](https://doi.org/10.1051/0004-6361/201525998)
- Chang, R. X., Hou, J. L., Shen, S. Y., & Shu, C. G. 2010, *ApJ*, 722, 380, doi: [10.1088/0004-637X/722/1/380](https://doi.org/10.1088/0004-637X/722/1/380)
- Chisholm, J., Tremonti, C. A., Leitherer, C., & Chen, Y. 2017, *MNRAS*, 469, 4831, doi: [10.1093/mnras/stx1164](https://doi.org/10.1093/mnras/stx1164)
- Cid Fernandes, R., Mateus, A., Sodré, L., Stasińska, G., & Gomes, J. M. 2005, *MNRAS*, 358, 363, doi: [10.1111/j.1365-2966.2005.08752.x](https://doi.org/10.1111/j.1365-2966.2005.08752.x)
- Clark, C. J. R., Schofield, S. P., Gomez, H. L., & Davies, J. I. 2016, *MNRAS*, 459, 1646, doi: [10.1093/mnras/stw647](https://doi.org/10.1093/mnras/stw647)
- De Vis, P., Gomez, H. L., Schofield, S. P., et al. 2017, *MNRAS*, 471, 1743, doi: [10.1093/mnras/stx981](https://doi.org/10.1093/mnras/stx981)
- De Vis, P., Jones, A., Viaene, S., et al. 2019, *A&A*, 623, A5, doi: [10.1051/0004-6361/201834444](https://doi.org/10.1051/0004-6361/201834444)
- Draine, B. T., & Salpeter, E. E. 1979, *ApJ*, 231, 438, doi: [10.1086/157206](https://doi.org/10.1086/157206)
- Draine, B. T., Dale, D. A., Bendo, G., et al. 2007, *ApJ*, 663, 866, doi: [10.1086/518306](https://doi.org/10.1086/518306)
- Edmunds, M. G. 2001, *MNRAS*, 328, 223, doi: [10.1046/j.1365-8711.2001.04859.x](https://doi.org/10.1046/j.1365-8711.2001.04859.x)
- Fitzpatrick, E. L., Massa, D., Gordon, K. D., Bohlin, R., & Clayton, G. C. 2019, *ApJ*, 886, 108, doi: [10.3847/1538-4357/ab4c3a](https://doi.org/10.3847/1538-4357/ab4c3a)
- Fu, J., Hou, J. L., Yin, J., & Chang, R. X. 2009, *ApJ*, 696, 668, doi: [10.1088/0004-637X/696/1/668](https://doi.org/10.1088/0004-637X/696/1/668)
- Galametz, M., Madden, S. C., Galliano, F., et al. 2011, *A&A*, 532, A56, doi: [10.1051/0004-6361/201014904](https://doi.org/10.1051/0004-6361/201014904)
- Galliano, F. 2022, Habilitation Thesis, 1. <https://arxiv.org/abs/2202.01868>
- Hirashita, H. 1999, *ApJ*, 522, 220, doi: [10.1086/307621](https://doi.org/10.1086/307621)
- Hirashita, H., Tajiri, Y. Y., & Kamaya, H. 2002, *A&A*, 388, 439, doi: [10.1051/0004-6361:20020605](https://doi.org/10.1051/0004-6361:20020605)
- Issa, M. R., MacLaren, I., & Wolfendale, A. W. 1990, *A&A*, 236, 237
- James, A., Dunne, L., Eales, S., & Edmunds, M. G. 2002, *MNRAS*, 335, 753, doi: [10.1046/j.1365-8711.2002.05660.x](https://doi.org/10.1046/j.1365-8711.2002.05660.x)
- Kahre, L., Walterbos, R. A., Kim, H., et al. 2018, *ApJ*, 855, 133, doi: [10.3847/1538-4357/aab101](https://doi.org/10.3847/1538-4357/aab101)
- Katz, H., Laporte, N., Ellis, R. S., Devriendt, J., & Slyz, A. 2019, *MNRAS*, 484, 4054, doi: [10.1093/mnras/stz281](https://doi.org/10.1093/mnras/stz281)
- Kauffmann, G., Heckman, T. M., Tremonti, C., et al. 2003a, *MNRAS*, 346, 1055, doi: [10.1111/j.1365-2966.2003.07154.x](https://doi.org/10.1111/j.1365-2966.2003.07154.x)
- Kauffmann, G., Heckman, T. M., White, S. D. M., et al. 2003b, *MNRAS*, 341, 33, doi: [10.1046/j.1365-8711.2003.06291.x](https://doi.org/10.1046/j.1365-8711.2003.06291.x)
- Li, L., Shen, S., Hou, J., et al. 2017, *AJ*, 153, 88, doi: [10.3847/1538-3881/153/2/88](https://doi.org/10.3847/1538-3881/153/2/88)
- Li, Q., Narayanan, D., & Davé, R. 2019, *MNRAS*, 490, 1425, doi: [10.1093/mnras/stz2684](https://doi.org/10.1093/mnras/stz2684)
- Lisenfeld, U., & Ferrara, A. 1998, *ApJ*, 496, 145, doi: [10.1086/305354](https://doi.org/10.1086/305354)
- Liu, G., Calzetti, D., Kennicutt, Robert C., J., et al. 2013, *ApJ*, 772, 27, doi: [10.1088/0004-637X/772/1/27](https://doi.org/10.1088/0004-637X/772/1/27)
- Lu, J., Shen, S., Yuan, F.-T., et al. 2022, *ApJ*, 938, 139, doi: [10.3847/1538-4357/ac92e9](https://doi.org/10.3847/1538-4357/ac92e9)
- Ma, X., Hayward, C. C., Casey, C. M., et al. 2019, *MNRAS*, 487, 1844, doi: [10.1093/mnras/stz1324](https://doi.org/10.1093/mnras/stz1324)
- Mattsson, L., Andersen, A. C., & Munkhammar, J. D. 2012, *MNRAS*, 423, 26, doi: [10.1111/j.1365-2966.2012.20575.x](https://doi.org/10.1111/j.1365-2966.2012.20575.x)
- Mattsson, L., Gomez, H. L., Andersen, A. C., et al. 2014, *MNRAS*, 444, 797, doi: [10.1093/mnras/stu1228](https://doi.org/10.1093/mnras/stu1228)
- Neistein, E., van den Bosch, F. C., & Dekel, A. 2006, *MNRAS*, 372, 933, doi: [10.1111/j.1365-2966.2006.10918.x](https://doi.org/10.1111/j.1365-2966.2006.10918.x)
- Oey, M. S., Parker, J. S., Mikles, V. J., & Zhang, X. 2003, *AJ*, 126, 2317, doi: [10.1086/378163](https://doi.org/10.1086/378163)
- Pandya, V., Fielding, D. B., Anglés-Alcázar, D., et al. 2021, *MNRAS*, 508, 2979, doi: [10.1093/mnras/stab2714](https://doi.org/10.1093/mnras/stab2714)
- Peng, Y.-j., Lilly, S. J., Kovač, K., et al. 2010, *ApJ*, 721, 193, doi: [10.1088/0004-637X/721/1/193](https://doi.org/10.1088/0004-637X/721/1/193)
- Rémy-Ruyer, A., Madden, S. C., Galliano, F., et al. 2014, *A&A*, 563, A31, doi: [10.1051/0004-6361/201322803](https://doi.org/10.1051/0004-6361/201322803)
- Sánchez Almeida, J., & Sánchez-Menguiano, L. 2019, *ApJL*, 878, L6, doi: [10.3847/2041-8213/ab218d](https://doi.org/10.3847/2041-8213/ab218d)
- Santoro, F., Kreckel, K., Belfiore, F., et al. 2022, *A&A*, 658, A188, doi: [10.1051/0004-6361/202141907](https://doi.org/10.1051/0004-6361/202141907)
- Shen, S., Mo, H. J., White, S. D. M., et al. 2003, *MNRAS*, 343, 978, doi: [10.1046/j.1365-8711.2003.06740.x](https://doi.org/10.1046/j.1365-8711.2003.06740.x)

Silva, L., Granato, G. L., Bressan, A., & Danese, L. 1998, ApJ, 509, 103, doi: [10.1086/306476](https://doi.org/10.1086/306476)

Somerville, R. S., Gilmore, R. C., Primack, J. R., & Domínguez, A. 2012, MNRAS, 423, 1992, doi: [10.1111/j.1365-2966.2012.20490.x](https://doi.org/10.1111/j.1365-2966.2012.20490.x)

Tremonti, C. A., Heckman, T. M., Kauffmann, G., et al. 2004, ApJ, 613, 898, doi: [10.1086/423264](https://doi.org/10.1086/423264)

Wiseman, P., Schady, P., Bolmer, J., et al. 2017, A&A, 599, A24, doi: [10.1051/0004-6361/201629228](https://doi.org/10.1051/0004-6361/201629228)

Yajima, H., Shlosman, I., Romano-Díaz, E., & Nagamine, K. 2015, MNRAS, 451, 418, doi: [10.1093/mnras/stv974](https://doi.org/10.1093/mnras/stv974)

Zafar, T., & Watson, D. 2013, A&A, 560, A26, doi: [10.1051/0004-6361/201321413](https://doi.org/10.1051/0004-6361/201321413)